Analysis of Pol-InSAR coherence region parameters over a permafrost landscape

Paloma Saporta[a,b], Alberto Alonso-González[c], Irena Hajnsek[a,b]
[a] Microwaves and Radar Institute, German Aerospace Center, Germany
[b] Institute of Environmental Engineering, ETH Zürich, Switzerland
[c] Signal Theory and Communications Department, Universitat Politècnica de Catalunya, Spain

Abstract

The present study proposes an analysis of the Pol-InSAR coherence region parameters over a permafrost region in the Canadian Arctic. The coherence region extent, for instance, may be understood as the height spanned by the InSAR phase centre heights associated with all possible polarisations. The variations of this extent and of other coherence region parameters with frequency, vegetation type and season will be analysed.

1 Introduction

Permafrost regions cover about a quarter of the Northern hemisphere land surface. In particular in the Northern Arctic, these regions face rapid changes in hydrology, geomorphology and ecology owing to increasing air temperatures and changing precipitation regime. Degradations of the ground leading to the mobilisation of carbon in previously frozen soil is considered as a potential future source of greenhouse gas. The characteristics of the soil thermal regime cannot be directly observed with optical remote sensing data, and linking it to vegetation and soil properties is a challenging task [1]. Radar remote sensing, featuring waves penetrating through the snow cover and to some extent within the winter frozen ground, is therefore a valuable tool for the monitoring of permafrost and the retrieval of permafrost characteristic variables.

2 Data

2.1 DLR's PermASAR campaign

The German Aerospace Center (DLR) dedicated an F-SAR airborne campaign to the investigation of the interaction of radar waves with frozen grounds: the Permafrost Airborne SAR Experiment (PermASAR) [2]. In the frame of this campaign, two missions were conducted over several permafrost regions in Canada, in summer 2018 and winter 2019. They correspond to thawed and frozen states of the upper layer of the ground, respectively.

2.2 The Trail Valley Creek test site

This study focuses on acquisitions over a particular continuous permafrost region in the Canadian Artic: the Trail Valley Creek catchment. It is located at the Northern treeline in the Northwest Territories, and features gently rolling hills covered by tundra vegetation and some isolated trees as described in [1].

In summer, the upper layer of the ground is thawed, over a depth of several decimetres above the permafrost (perennially frozen ground) itself. In winter, the ground is entirely frozen and covered by several decimetres of snow, and the vegetation is mostly frozen.

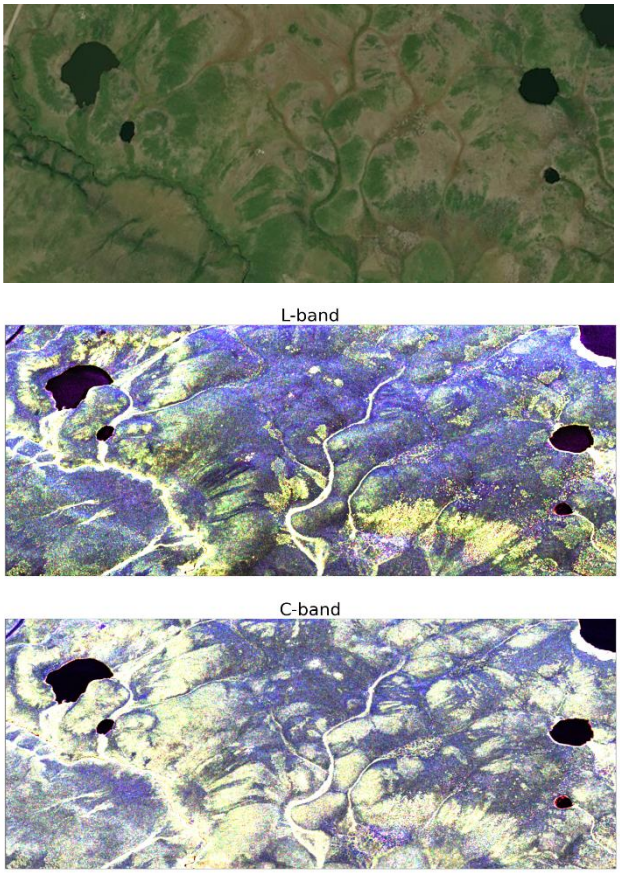

Figure 1 The focus region at Trail Valley Creek (Canada). The upper figure is an optical image from QGIS basemap, the two lower figures are the Pauli images corresponding to summer 2018 at L and C-band, respectively.

At the Trail Valley Creek test site, the F-SAR instrument onboard DLR's research plane was operated at three frequencies, X, C and L-band, and fully polarimetric images were acquired. Several baselines were flown by the plane, allowing for interferometric processing. The simultaneous occurrence of InSAR and PolSAR frameworks allows to retrieve Pol-InSAR observables. We propose here the analysis of such observables for a single baseline, of respectively 100 m at L-band and 25 m at C-band, leading to a similar vertical wavenumber, which averages to 1 rad/m within the scene.

Additional data acquired by the Alfred Wegener Institute with airborne Lidar over the same site is used as reference information. In particular, the high-resolution Digital Terrain Model [3] is used to correct for the InSAR topographic phase, and vegetation height [3] and landcover [4] products are used to assess the Pol-InSAR observables.

3 Method

The Pol-InSAR coherence region can be characterized by its extent in norm and in phase. The extent in phase translated to an extent in height corresponds to the height difference spanned by the interferometric phase centre heights at all possible polarisations.

For each SAR pixel, from the two coherency matrices T_{11} and T_{22}, and the matrix Ω_{12} containing the Pol-InSAR information, let us define [5]

$$\Pi = T_M^{-1/2} \Omega_{12} T_M^{-1/2}$$

where $T_M = 1/2(T_{11} + T_{22})$. The Pol-InSAR coherence region can be approximated by the field of value of the matrix Π. The latter can be characterized using the polar decomposition of Π [6]: the matrix Π is decomposed as

$$\Pi = UP$$

where $P = (\Pi^{*T}\Pi)^{1/2}$ is a positive semi-definite hermitian matrix, and $U = \Pi P^{-1}$ is a unitary matrix. From the eigenvectors $(v_i)_{i=1,2,3}$ of U, the associated coherences in the coherence region are retrieved as $\gamma_i = v_i^{*T}\, \Pi v_i$. The angular extent of the coherence region can then be approximated by

$$\Delta\phi = max\{|\phi_i - \phi_j|\}$$

where $\{\phi_i\}_{i=1,2,3}$ are the phases of the previous coherences: $\phi_i = arg(\gamma_i)$. The extent in angle $\Delta\phi$ is then transferred to an extent in height by means of the vertical wavenumber κ_z associated with the considered baseline: $\Delta h = \Delta\phi/\kappa_z$. Similarly, the coherences associated with the eigenvalues of P relate to the norm extent $\Delta|\gamma|$ of the coherence region. A visualization of these parameters may be seen in **Figure 2**.

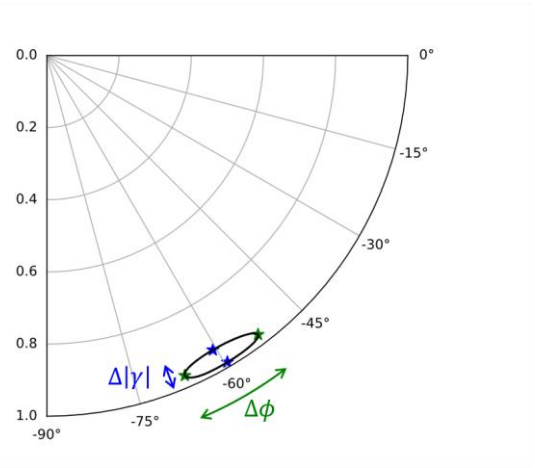

Figure 2 Example of phase optimisation for a single pixel. The coherence region boundary is plotted in black. The green stars correspond to the phase optimised coherences, their maximum extent in phase $\Delta\phi$ is indicated by the green arrow. Similarly, the blue stars correspond to the norm optimised coherences, their maximum extent in norm $\Delta|\gamma|$ is indicated by the blue arrow.

4 Results and discussion

This study focuses on a smaller region of the test site located in the vicinity of the Trail Valley Creek Research station. Optical imagery over this region is shown on **Figure 1**. The Pol-InSAR coherence region phase and norm extents are computed pixelwise for a given acquisition pair, and analysed with respect to frequency, season and vegetation type. The vegetation height and classes on the considered region are shown on **Figure 3**.

4.1 Coherence region phase extent

Figure 4 shows the coherence region extent in phase, translated to height difference in meters, at L and C-band for summer and winter acquisitions. The associated histograms are shown on **Figure 5**.

At L-band in summer, the coherence regions show an overall increase in phase extent with the vegetation height, which is increasing from left to right according to the vegetation types. The height extent of pixels classified as trees

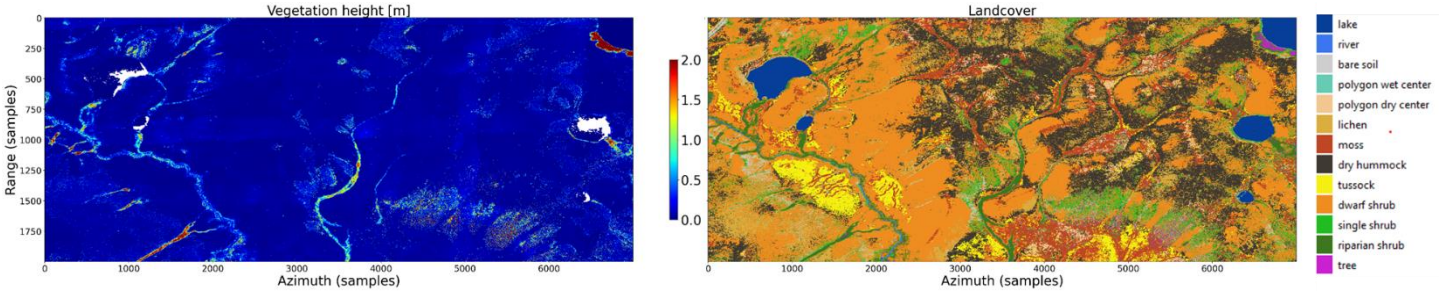

Figure 3 Lidar vegetation height (left) and landcover classification (right) over the region, in the radar geometry

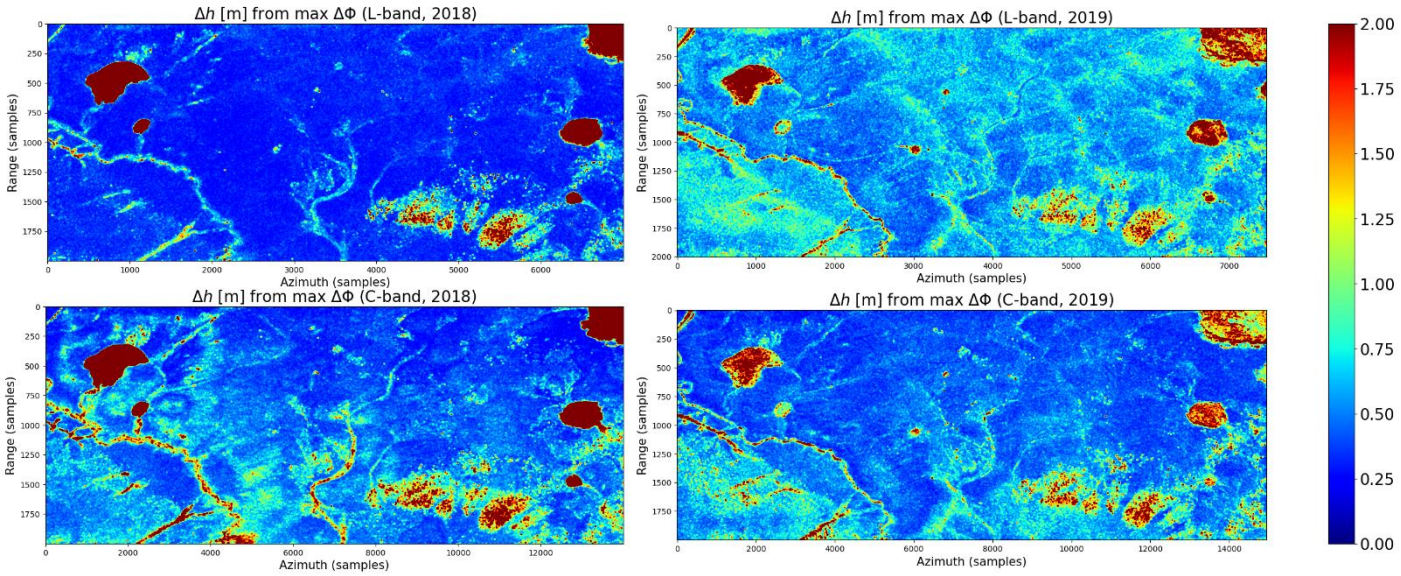

Figure 4 Coherence region phase extent, translated into height extent [m] (left: summer, right: winter) in the radar geometry. The upper row shows L-band result, the lower row C-band results. Maximum filtering on a 5m by 5m square window has been performed in order to enhance spatial features.

is smaller than the Lidar reference, which is expected as the radar signal penetrates the whole canopy and the phase centre height obtained will be somewhere within the canopy extent for all polarizations. Short vegetation types are overestimated with respect to the Lidar reference, which means that the extent spanned by the interferometric phase centre heights at all possible polarisations is larger than the vegetation height. This cannot be explained by the penetration of the radar wave into the thawed ground as it is supposed to be small. Indeed, the soil is, according to the ground measurements, humid as the permafrost table acts like an impermeable layer. The larger height could then be due to either an overestimation of the phase extent linked to the phase error associated with the coherences, or to a small underestimation of the vegetation height in case the Lidar wave does not penetrate through dense vegetation until the ground.

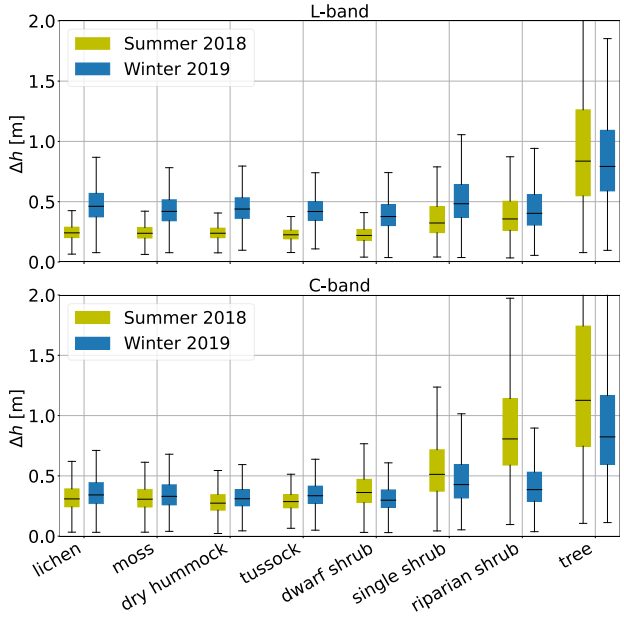

Figure 5 Boxplots of coherence region phase extent, translated to [m] in summer 2018 and winter 2019 for the most relevant vegetation types. Top and bottom figures correspond respectively to L and C-band. Vegetation types are ordered with overall increasing vegetation height.

In winter, the height extent of trees decreases, which can be explained by the fact that partially frozen trees become more transparent to the radar due to the drop of dielectric constant, therefore the observed reduced scattering. On the other hand, the height extent of shorter vegetation increases compared to summer, reaching in average more than 50 cm. This can be explained either by the expected penetration of radar waves into frozen ground, leading to an increased volume decorrelation. Indeed, as the interferometric pairs have been corrected for range spectral filtering, the remaining coherence ideally only depends on the volume decorrelation term [5].

At C-band, **Figure 4** suggests that the difference between summer and winter phase extents is smaller than at L-band. This is confirmed on the boxplots of **Figure 5** for short vegetation types. It is interesting to note that the taller vegetation types see a decrease in their phase extent at C-band. This could be explained also by the vegetation being more transparent for radar waves when it is frozen (in winter).

4.2 Coherence region norm extent

Figure 6 features the coherence region extent in norm at L and C-band for summer and winter acquisitions. The associated histograms are shown on **Figure 7**.
For all season and band combinations, the coherence region extent in norm reveals similar spatial patterns than the height extent. In this regard, the coherence region norm

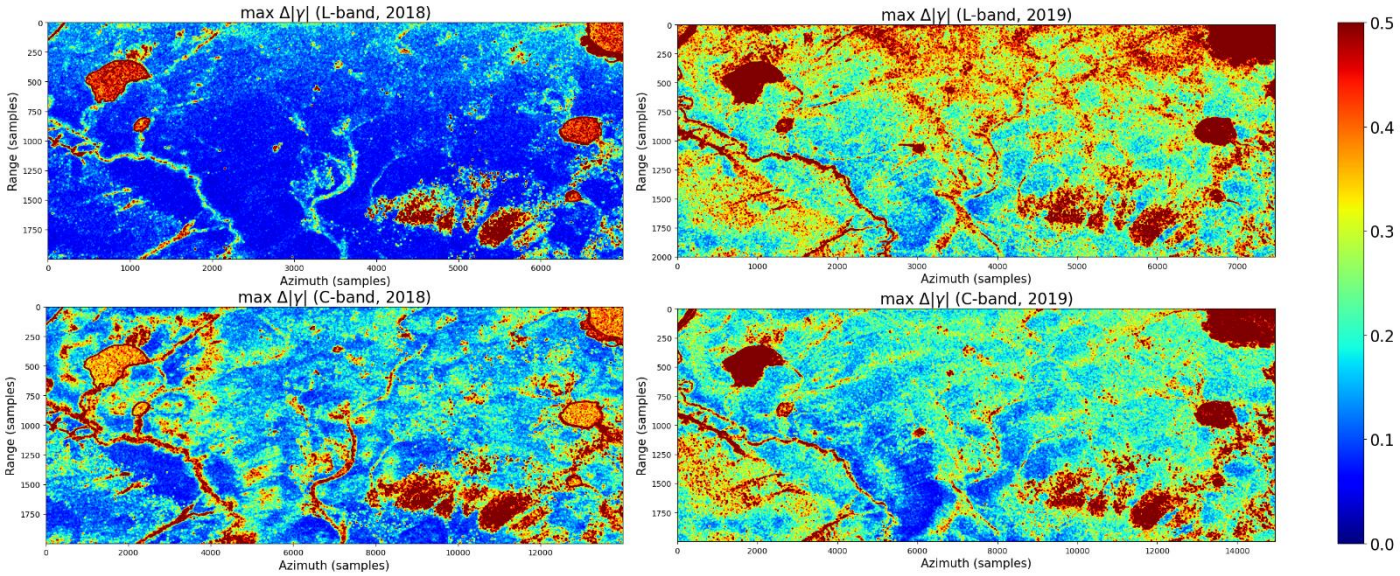

Figure 6 Coherence region norm extent (left: summer, right: winter) in the radar geometry. The upper row features L-band result, the lower row C-band results. Maximum filtering on a 5m by 5m square window has been performed in order to enhance spatial features.

extent in summer increases when the vegetation height increases. There is as well less difference in winter, compared to summer, in-between vegetation classes at L-band. This means that the vegetation type is not an explicative factor of the coherence region amplitudes in winter.
It can be noted that at for short vegetation classes, there are larger differences between summer and winter when considering the coherence region norm extent than its height extent.

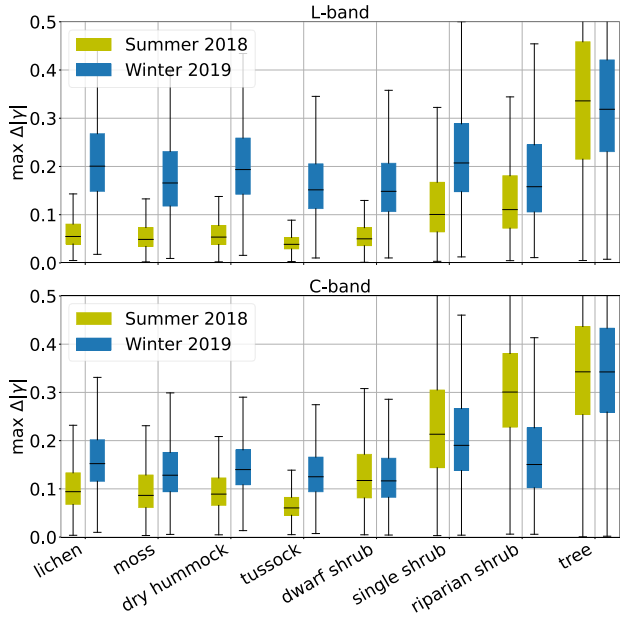

Figure 7 Boxplots of coherence region norm extent in summer 2018 and winter 2019 for the most relevant vegetation types. Top and bottom figures correspond respectively to L and C-band. Vegetation types are ordered with overall increasing vegetation height.

5 Summary

To sum up, in summer the coherence region shape parameters at a given pixel are related to the landcover. In winter, the coherence region phase extent is larger than in summer, and relatively independent from vegetation type, suggesting a possible influence of penetration into the frozen upper soil.
This analysis shows that Pol-InSAR coherence region shapes and more generally Pol-InSAR multifrequency observables are a valuable tool to characterize permafrost scenes.

6 Acknowledgements

We would like to thank Julia Boike and Inge Grünberg (Alfred Wegener Institute) for sharing their vegetation classification map over the Trail Valley Creek.

7 Literature

[1] I. Grünberg, E.J. Wilcox, S. Zwieback, P. Marsh, and J. Boike, “Linking tundra vegetation, snow, soil temperature, and permafrost”, Biogeosciences, 17(16), 4261-4279, 2020.

[2] I. Hajnsek, H. Joerg, R. Horn, M. Keller, D. Gesswein, M. Jaeger, R. Scheiber, P. Bernhard, S. Zwieback, “DLR Airborne SAR Campaign on Permafrost Soils and Boreal Forests in the Canadian Northwest Territories, Yukon and Saskatchewan: PermASAR”, POLINSAR 2019; 9th International Workshop on Science and Applications of SAR Polarimetry and Polarimetric Interferometry, 2019

[3] S. Lange, I. Grünberg, K. Anders, J. Hartmann, V. Helm and J. Boike, “Airborne Laser Scanning (ALS)

Point Clouds of Trail Valley Creek, NWT, Canada (2018)", PANGAEA, https://doi.org/10.1594/PANGAEA.934387, 2021

[4] I. Grünberg et al., work in progress, 2023

[5] S. Cloude, "Polarisation: applications in remote sensing", OUP Oxford, 2009

[6] N.J. Higham, "Computing the polar decomposition—with applications", SIAM Journal on Scientific and Statistical Computing, 7(4), 1160-1174, 1986